

# Gone with the wind: Where is the missing stellar wind energy from massive star clusters?

Anna L. Rosen,<sup>1</sup>★ Laura A. Lopez,<sup>2</sup>† Mark R. Krumholz<sup>1</sup> and Enrico Ramirez-Ruiz<sup>1</sup>

<sup>1</sup>*Department of Astronomy and Astrophysics, University of California, Santa Cruz, CA 95064 USA*

<sup>2</sup>*MIT-Kavli Institute for Astrophysics and Space Research, 77 Massachusetts Avenue, 37-664H, Cambridge, MA 02139, USA*

Accepted 2014 May 23. Received 2014 May 23; in original form 2014 May 6

## ABSTRACT

Star clusters larger than  $\sim 10^3 M_{\odot}$  contain multiple hot stars that launch fast stellar winds. The integrated kinetic energy carried by these winds is comparable to that delivered by supernova explosions, suggesting that at early times winds could be an important form of feedback on the surrounding cold material from which the star cluster formed. However, the interaction of these winds with the surrounding clumpy, turbulent, cold gas is complex and poorly understood. Here, we investigate this problem via an accounting exercise: we use empirically determined properties of four well-studied massive star clusters to determine where the energy injected by stellar winds ultimately ends up. We consider a range of kinetic energy loss channels, including radiative cooling, mechanical work on the cold interstellar medium, thermal conduction, heating of dust via collisions by the hot gas, and bulk advection of thermal energy by the hot gas. We show that, for at least some of the clusters, none of these channels can account for more than a small fraction of the injected energy. We suggest that turbulent mixing at the hot–cold interface or physical leakage of the hot gas from the H II region can efficiently remove the kinetic energy injected by the massive stars in young star clusters. Even for the clusters where we are able to account for all the injected kinetic energy, we show that our accounting sets strong constraints on the importance of stellar winds as a mechanism for feedback on the cold interstellar medium.

**Key words:** radiation mechanisms: thermal – ISM: bubbles – H II regions – ISM: kinematics and dynamics – X-rays: ISM.

## 1 INTRODUCTION

Massive star clusters (MSCs;  $M_{\star} \gtrsim 10^3 M_{\odot}$ ) are born in the dense regions of giant molecular clouds (GMCs). The resulting injection of energy and momentum by the young stars (i.e. stellar feedback) terminates star formation and expels gas from the MSC. These feedback processes are likely responsible for the low star formation efficiencies observed in GMCs (Matzner & McKee 2000; Krumholz & Tan 2007), they control the dynamics of the H II regions surrounding these young clusters (Krumholz & Matzner 2009; Lopez et al. 2011, 2013b), and they may be responsible for the dissolution and ultimate disruption of their host molecular clouds. For recent reviews, see Krumholz et al. (2014) and Krumholz (2014).

Newborn stars in these clusters dramatically affect the surrounding interstellar medium (ISM) via photoionization flows (e.g. Dale, Ercolano & Bonnell 2013), direct stellar radiation pressure (e.g. Krumholz & Matzner 2009; Fall, Krumholz & Matzner 2010; Murray, Quataert & Thompson 2010), dust-reprocessed radia-

tion pressure (e.g. Thompson, Quataert & Murray 2005; Murray, Quataert & Thompson 2010), protostellar outflows (e.g. Cunningham et al. 2011), and hot gas shock-heated by stellar winds (e.g. Castor, McCray & Weaver 1975; Weaver et al. 1977; Cantó, Raga & Rodríguez 2000; Stevens & Hartwell 2003; Harper-Clark & Murray 2009) and supernovae (SNe; e.g. McKee & Ostriker 1977; Chevalier & Clegg 1985). The expansion of a cool, dense shell of interstellar material surrounding the H II region is driven by these processes (Castor et al. 1975; Weaver et al. 1977; McKee & Ostriker 1977; Krumholz & Matzner 2009).

It is still uncertain which of these processes dominate stellar feedback and thus drive the subsequent expansion of the H II region shell. Recent studies of H II regions which host MSCs suggest that the thermal pressure of the warm ( $\sim 10^4$  K) ionized gas dominates H II region dynamics at late times, while radiation pressure may dominate during H II regions' infancy (for  $R_{\text{HII}} \lesssim 1\text{--}100$  pc; Krumholz & Matzner 2009; Fall et al. 2010; Lopez et al. 2011, 2013b). However, the importance of stellar winds remains uncertain (Lopez et al. 2011, 2013b; Pellegrini, Baldwin & Ferland 2011; Rogers & Pittard 2013). The total energy injected by stellar winds is quite large for MSCs (Kudritzki et al. 1999; Repolust, Puls & Herrero 2004), but whether this energy contributes significantly to

\* E-mail: [alrosen@ucsc.edu](mailto:alrosen@ucsc.edu)

† NASA Einstein Fellow, Pappalardo Fellow in Physics.

the dynamics of the shell, or if most of it escapes or is radiated away, remains unresolved.

Massive stars have mass-loss rates on the order of  $\dot{M}_w \sim 10^{-6} M_\odot \text{ yr}^{-1}$  (Repolust et al. 2004). This mass escapes the stellar surface at velocities of  $v_w \sim 1000 \text{ km s}^{-1}$  (Leitherer, Robert & Drissen 1992), resulting in an energy injection rate of  $(1/2)\dot{M}_w v_w^2 \sim 100 L_\odot$  per massive star. In an MSC, these fast stellar winds collide with the winds of nearby stars, producing multiple shocks with complex morphologies. The hot, collective stellar wind will then produce an outward-directed ‘cluster wind’ as the hot gas adiabatically expands and ultimately leaves the cluster (Cantó et al. 2000; Stevens & Hartwell 2003). The resulting ‘super-bubble’ (Bruhweiler et al. 1980) fills the surrounding H II region with hot, shocked stellar wind material at temperatures of  $\sim 10^7 \text{ K}$ , and produces diffuse X-ray emission. This X-ray emission has been detected from numerous MSCs in the Milky Way (MW; Moffat et al. 2002; Townsley et al. 2003, 2006, 2011b) and the Large Magellanic Cloud (LMC; Lopez et al. 2011, 2013b).

While the source of the X-ray emission is well understood, its luminosity is not: the X-ray luminosity of H II regions associated with MSCs is less than expected if the kinetic energy supplied by winds was retained within the super-bubbles. There are several competing theoretical models to account for the X-ray luminosity in bubbles around MSCs, and these models imply different dynamical importance for stellar winds (and SNe, which also produce shocked hot gas). Castor et al. (1975) and Weaver et al. (1977) assume that the hot gas in the bubble is fully confined by a cool shell expanding into a uniform density ISM, whereas Chevalier & Clegg (1985) ignore the surrounding ISM and simply assume a steady, freely expanding wind. Compared to observations of M17 (Townsley et al. 2003), the Carina Nebula (Townsley et al. 2011a), and 30 Doradus (30 Dor; Townsley et al. 2006; Lopez et al. 2011), the models of Castor et al. (1975) and Weaver et al. (1977) overpredict the observed X-ray luminosity, while that of Chevalier & Clegg (1985) underpredicts it (Dunne et al. 2003; Harper-Clark & Murray 2009; Lopez et al. 2011). This result led Harper-Clark & Murray (2009) to introduce an intermediate model, where the hot gas expands into a non-uniform ISM, producing a ‘porous’ shell from which the hot gas can leak. This model is capable of fitting the observed X-ray luminosities, but the porosity is treated as a free parameter, not independently predicted.

The model of Harper-Clark & Murray assumes the low X-ray luminosities are caused by hot gas leakage, but there are several other channels by which the wind energy can be lost. One possibility is that hot and cold gas may also exchange energy via laminar or turbulent conduction; the latter process occurs when turbulence at the hot–cold interface produces small-scale mixing of hot and cold gas, greatly accelerating conductive transfer between the two (McKee, van Buren & Lazareff 1984; Strickland & Stevens 1998; Nakamura et al. 2006). A closely related possibility is that turbulence at the hot–cold interface mixes dust grains into the hot gas, or that dust is produced *in situ* within the super-bubble by evolved stars. Dust grains immersed in hot gas will eventually be destroyed by sputtering, but they will absorb thermal energy and radiate it in the IR before that. A final possibility is that the hot gas can transfer energy to the ISM by doing mechanical work on the cold, dense shell that bounds the H II region, leading to either coherent or turbulent motions (Breitschwerdt & Kahn 1988).

As previously mentioned, the effect of leakage is intimately tied to the question of stellar wind feedback in MSC formation. The contribution of stellar winds to H II region dynamics, and their importance as a mechanism for limiting star formation efficiencies,

depend on how much of the stellar wind energy is used to do work on the cold ISM, and how much energy is transferred to other channels. In this paper, we attempt to determine this division of energy through observations. We examine four well-studied H II regions (30 Doradus, Carina, NGC 3603, and M17), and we evaluate how the energy stored in the hot gas is lost via these different mechanisms using X-ray observations coupled to ancillary radio data. By conducting this energy census, we estimate the wind energy which leaks from the H II shells, and we explore the implications regarding the role of stellar winds in regulating star formation in MSCs. This paper is organized as follows: Section 2 presents the theoretical framework by reviewing the many different avenues the hot X-ray emitting gas can lose energy. Section 3 discusses our source selection criteria and describes our resulting MSC sample. We present the results of our analysis of these regions in Section 4, and discuss their implications in Section 5. Finally, we summarize and conclude our analysis in Section 6.

## 2 THEORY AND BACKGROUND: ENERGY BUDGETS

### 2.1 $L_w$ : energy injection by stellar winds

Consider an idealized, simple spherical H II region with an MSC at its centre, injecting wind energy at a rate of

$$L_w = \sum_{i=1}^N \frac{1}{2} \dot{M}_{w,i} v_{w,i}^2, \quad (1)$$

where  $\dot{M}_{w,i}$  and  $v_{w,i}$  are the mass-loss rate and wind velocity for star  $i$ , and  $N$  is the total number of massive stars in the MSC. For typical MSCs in the MW and LMC,  $L_w$  has values of  $\sim 10^{37}–10^{39} \text{ erg s}^{-1}$  (Crowther & Dessart 1998; Dunne et al. 2003; Smith 2006; Doran et al. 2013). The region has a radius  $R$ , and is bounded by a shell of cold, dense material expanding at velocity  $v_{sh}$ . It is filled with hot gas with temperature  $T$  and electron number density  $n_X$ . We assume that its filling factor is unity to assess the global dynamical effect of the hot gas on the shell (Lopez et al. 2011). This picture is an oversimplification of the structure of a real H II region around an MSC. However, as we shall see below, the missing wind energy is so large that even this simplified model is able to provide meaningful constraints on the missing kinetic energy carried by stellar winds.

For the purposes of this study, we only consider the energy injected by stellar winds and ignore the contribution by SNe. This assumption is reasonable for the following reasons. First, all of the H II regions considered in this paper have young MSCs (of ages  $\sim 1–3 \text{ Myr}$ ) so that SNe have not occurred yet. Secondly, the mechanical energy of one SN ( $\sim 10^{51} \text{ erg}$ ) is comparable to the amount injected by winds over a single massive star’s lifetime (Castor et al. 1975). As a result, ignoring SNe amounts to, at most, a factor of 2 error in the total kinetic energy injection. Finally, as we demonstrate later, we cannot account for the total energy injection by winds alone. Including the heating contribution from SNe would only strengthen our conclusions. Therefore, by using the observed X-ray, stellar population, and kinematic properties of several H II regions, we examine the possible avenues that the hot gas can transfer energy in these H II regions. From our analysis, we determine which processes, if any, can account for the missing kinetic energy. The remainder of this section discusses the various energy sinks for the hot gas.

## 2.2 $L_{\text{cool}}$ : radiative cooling of the hot gas

The energy injected by winds can be lost via several channels, the first of which is radiative cooling. The hot gas cools primarily via thermal bremsstrahlung and metal-line cooling. An optically thin ‘parcel’ of hot gas with volume  $dV$  and electron and ion number densities of  $n_X$  and  $n_i$ , respectively, loses energy via radiation at a rate

$$dQ = -n_X n_i \Lambda(T, x_i, Z) dV dt, \quad (2)$$

where  $\Lambda(T, x_i, Z)$  is the radiative cooling function (with units of  $\text{erg s}^{-1} \text{cm}^3$ ), which depends on the temperature  $T$ , ionization state  $x_i$ , and metallicity  $Z$  of the hot gas. For a fully ionized plasma of solar composition,  $n_i = 0.9 n_X$ . Since  $n_X$  is dominated by the free electrons liberated from H and He, the ratio of  $n_i/n_X$  is nearly identical for the LMC and MW sources. For a low-density, optically thin plasma,  $\Lambda(T, x_i, Z)$  is independent of density. We use CHIANTI (Dere et al. 1997) to calculate  $\Lambda(T, x_i, Z)$  for MW and LMC metallicities, as shown in Fig. 1 (Russell & Dopita 1992; Grevesse & Sauval 1998). The ionization state is determined by assuming the plasma is in collisional ionization equilibrium (CIE; we discuss deviations from CIE in Section 5.1), and that charge exchange, radiative recombination, and dielectronic recombination are the only processes altering the ionization balance (Draine 2011). In this case, the ionization fractions,  $x_i$ , depend only on the gas temperature, and hence  $\Lambda$  only depends on  $T$  and  $Z$ . Under these assumptions, the total energy loss rate via cooling is

$$L_{\text{cool}} = 0.9 n_X^2 \Lambda(T, Z) V, \quad (3)$$

where  $V$  is the H II region volume. For typical shocked gas temperatures of H II regions ( $\sim 10^7$  K), most of the photons produced by this cooling have  $\sim$  keV energies, and thus are observable with X-ray telescopes, such as the *Chandra* X-ray Observatory.

We can use this result to place a constraint on the number density of the hot gas, since  $L_{\text{cool}} \propto n_X^2$ . If we assume that radiative cooling is the sole mechanism responsible for removing the kinetic energy

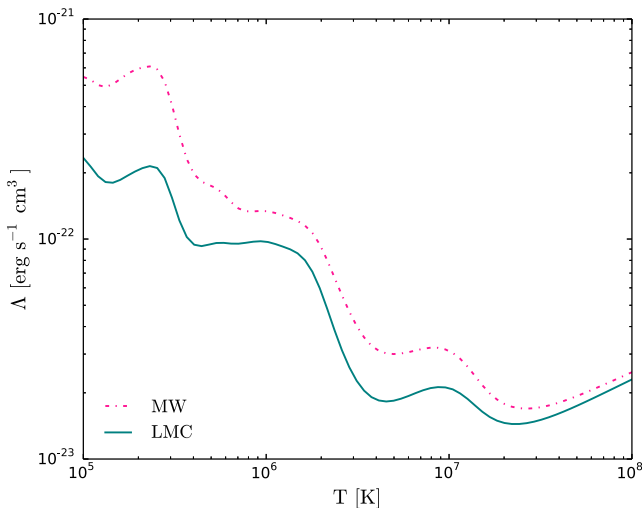


**Figure 1.** Radiative cooling functions from CHIANTI for MW ( $Z = Z_{\odot}$ ; pink dash-dotted line) and LMC ( $Z = 0.5 Z_{\odot}$ ; teal solid line) metallicities assuming that the hot gas is in CIE.

injected by winds (i.e.  $L_{\text{cool}} = L_w$ ), then the electron density of the hot gas is

$$n_{\text{cool}} = \sqrt{\frac{L_w}{0.9 \Lambda(T) V}}. \quad (4)$$

To illustrate our calculation, we consider two example H II regions with radii of 25 and 50 pc, respectively. Fig. 2 shows the value of  $n_{\text{cool}}$  versus temperature (solid teal line) for these two example regions, using a kinetic energy input rate of  $L_w = 10^{38} \text{ erg s}^{-1}$ . Energy conservation requires that the hot gas density and temperature must be at or below the  $n_{\text{cool}}$  versus  $T$  curve, since the gas cannot radiate more energy than is injected by stellar winds. The shaded region above the  $n_{\text{cool}}$  line denotes the disallowed region and highlights the combinations of thermodynamic properties that violate energy conservation.

## 2.3 $L_{\text{mech}}$ : mechanical work on the dense shell

The second channel by which the hot gas can transfer energy is by doing mechanical work on the cooler gas around it – either the cold neutral ISM, or the warm ( $\sim 10^4$  K) gas produced by photoionization. Observations of H II regions show that they are generally undergoing coherent expansion at speeds comparable to or larger than their internal turbulent velocities (e.g. Balick, Boeshaar & Gull 1980; Clayton et al. 1985), so we can think of this process as the hot gas acting as a piston pushing on a dense shell bounding the H II region. The thermal pressure of the hot gas is given by  $P_X = 1.9 n_X k_B T$ , and the rate at which this pressure does work  $W$  on the surrounding shell is  $dW/dt = 4\pi R^2 P_X v_{\text{sh}}$ . The factor of 1.9 arises from the fact that the total number density (e.g.  $n = n_i + n_X$ ) contributes to the pressure, and we have assumed that  $n_X = 0.9 n_i$ . We note that  $P_X = \frac{2}{3} u_X$  where  $u_X$  is the energy density of the hot gas and  $4\pi R^2 v_{\text{sh}}$  is the rate that the volume increases as the H II region expands. Under these assumptions, the rate at which the hot gas does work on the bubble shell is

$$L_{\text{mech}} = 7.6 \pi R^2 v_{\text{sh}} n_X k_B T. \quad (5)$$

Note that it does not matter whether this work is being done on  $10^4$  K photoionized gas,  $\sim 100$  K cold neutral gas, or some combination of the two, so long as the working surface at the hot–cold interface is roughly  $4\pi R^2$ , and the pressure of the hot gas greatly exceeds that of the cooler gas on which it is pushing. If the latter does not hold and the pressure of the cooler gas is actually greater than that of the hot gas, then the direction of energy flow will be reversed (i.e. the cold gas will do mechanical work on the hot gas), and our estimate of  $L_{\text{mech}}$  will be an upper limit.

As with radiative cooling, we can obtain an upper limit on the electron density by considering the highest value that it could have without the resulting work exceeding the available kinetic energy supply provided by the winds (i.e.  $L_{\text{mech}} = L_w$ ). We find that the maximum allowed number density of the hot gas is given by

$$n_{\text{mech}} = \frac{L_w}{7.6 \pi R^2 v_{\text{sh}} k_B T}, \quad (6)$$

which is also shown in Fig. 2 (dot-dashed pink line). For this example, we take  $v_{\text{sh}} = 20 \text{ km s}^{-1}$  which is typical for young H II regions (e.g. see Table 1). Similarly, since  $L_{\text{mech}}$  increases with increasing  $n_X$ , the hot gas is only allowed to have number densities less than or equal to  $n_{\text{mech}}$ . This result places another constraint on  $n_X$ , and produces another disallowed region in the  $n_X$ – $T$  plane.

We note that for temperatures below  $\sim 10^6$  K, all wind energy is lost via radiation. At temperatures above a  $\sim \text{few} \times 10^6$  K,

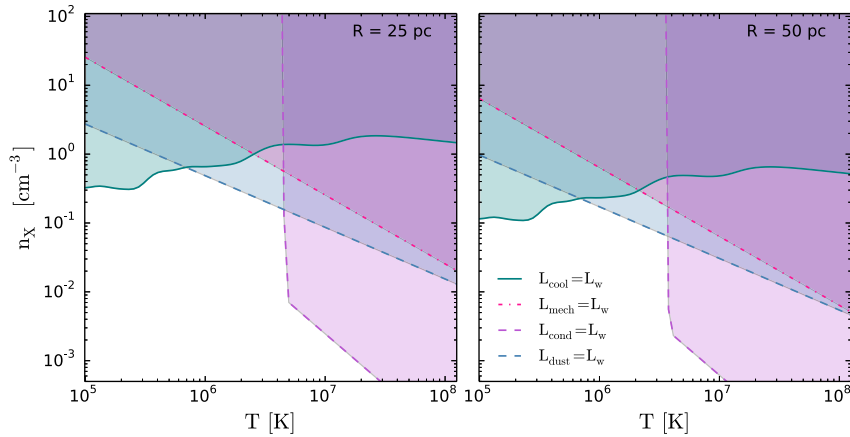


**Figure 2.** Allowed number densities and temperatures (white regions) for the plasma filling simulated H II regions with radii of 25 pc (left-hand panel) and 50 pc (right-hand panel), respectively. We take  $L_w = 10^{38} \text{ erg s}^{-1}$  and  $v_{\text{sh}} = 20 \text{ km s}^{-1}$ . Curves denote the loci in the  $T$ – $n_X$  plane where each of the energy sinks discussed in Section 2 are capable of removing all of the energy injected by winds. Shaded regions denote values of  $n_X$  and  $T$  that are disallowed because the energy loss rate exceeds the energy input rate.

**Table 1.** Table of the H II region properties in our sample. Properties listed are distance, H II region radius, shell velocity, MSC age, bolometric luminosity, integrated wind luminosity, observed unabsorbed X-ray luminosity, and spectral fitted temperatures for the hot X-ray emitting gas.

Name	$D$ (kpc)	$R_{\text{sh}}$ (pc)	$v_{\text{sh}}$ (km s $^{-1}$ )	$t_{\text{cl}}$ (Myr)	$\log L_{\text{bol}}$ ( $L_{\odot}$ )	$L_w$ ( $10^{37} \text{ erg s}^{-1}$ )	$L_x$ ( $10^{35} \text{ erg s}^{-1}$ )	$T_X$ ( $10^6 \text{ K}$ )
30 Doradus	50	100	25	2	8.4	224	45.0	7.4
Carina	2.3	20	20	3	7.23	35.0	1.71	4.5 <sup>a</sup>
NGC 3603	7.0	21	20	1	–	62.0	2.6	6.2 <sup>a</sup>
M17	2.1	5.8	25	1	6.58	1	0.2	5.3 <sup>a</sup>

<sup>a</sup>Temperatures shown are surface-brightness-weighted values from Townsley et al. (2011b).

References – *30 Doradus*: Lopez et al. (2011), Doran et al. (2013), Lopez et al. (2013b); *Carina*: Smith et al. (2000), Smith (2006), Smith & Brooks (2007), Harper-Clark & Murray (2009), Townsley et al. (2011b); *NGC 3603*: Balick et al. (1980), Crowther & Dessart (1998), Townsley et al. (2011b), *M17*: Clayton et al. (1985), Dunne et al. (2003), Townsley et al. (2003), Hoffmeister et al. (2008), Townsley et al. (2011b).

mechanical work is more effective than cooling at removing the wind energy. This transition is easily discerned by calculating the ratio

$$\frac{L_{\text{cool}}}{L_{\text{mech}}} = 0.16 \frac{\Lambda(T, Z) \Sigma_X}{k_B T v_{\text{sh}}}, \quad (7)$$

where  $\Sigma_X = n_X R$  is the surface density of the hot gas. This ratio is less than unity for temperatures where  $n_{\text{mech}} < n_{\text{cool}}$ .

#### 2.4 $L_{\text{cond}}$ : thermal conduction

Conduction is a third possible kinetic energy sink. In the absence of magnetic fields, thermal conduction by the hot electrons can be an efficient energy loss mechanism at the inner edge of the cool bubble shell, since the conductive heat flux from a fully ionized plasma depends sensitively on temperature ( $\propto T^{7/2}$ , Spitzer 1962). This process creates a region of intermediate temperature gas ( $T \sim 10^5 \text{ K}$ ) between the hot bubble interior and the cold shell, and this region will shed energy rapidly via metal-line cooling in the far-UV. This light would be extremely difficult to detect observationally, due to the high opacity of the ISM at these wavelengths and the even greater opacity of the Earth’s atmosphere.

For classical conductivity, the heat flux is  $q_c = -\kappa_c \nabla T$ , where

$$\kappa_c = 0.87 \frac{k_B^{7/2} T^{5/2}}{m_e^{1/2} e^4 \ln \Lambda_C} \quad (8)$$

is the thermal conductivity of the hot electrons with temperature  $T$ , and

$$\ln \Lambda_C = 29.7 + \ln \left( n_X^{-1/2} \frac{T}{10^6 \text{ K}} \right) \quad (9)$$

is the Coulomb logarithm for  $T > 4.2 \times 10^5 \text{ K}$  (Spitzer 1962; Cowie & McKee 1977; Draine 2011). Cowie & McKee (1977) find that when the electron mean free path becomes comparable to or greater than the temperature scaleheight,  $T/|\nabla T|$ , the heat flux saturates and takes on the value

$$q_s = 0.4 \left( \frac{2k_B T}{\pi m_e} \right)^{1/2} n_X k_B T. \quad (10)$$

The total energy loss rate due to conduction for an H II region with radius  $R$  filled with hot gas at a temperature  $T$  is therefore

$$L_{\text{cond}} = 4\pi R^2 \min(\kappa_c |\nabla T|, q_s). \quad (11)$$

We further assume that  $|\nabla T| \sim T/R$ , which is true at the order of magnitude level.

If thermal conduction is responsible for removing the bulk of the energy injected by stellar winds ( $L_{\text{cond}} = L_w$ ), then the required number density of the hot gas is

$$n_{\text{cond}} = \left( \frac{T}{10^6 \text{ K}} \right)^2 \exp \left( 59.4 - 6.96\pi \frac{k_B^{7/2} T^{7/2} R}{m_e^{1/2} e^4 L_w} \right), \quad (12)$$

assuming that the heat flux is not saturated. This result follows from equations (8), (9) and (11). However, if the temperature is large

enough such that the conductive heat-flux becomes saturated, then the number density required for conduction to dominate the energy loss is

$$n_{\text{cond}} = \left(\frac{m_e}{2\pi}\right)^{1/2} \frac{L_w}{1.6R^2 k_B^{3/2} T^{3/2}}, \quad (13)$$

which follows from equations (10) and (11). These results are also shown in Fig. 2 (purple dashed line). The shaded region to the right of this curve denotes the forbidden region where conductive losses exceed wind energy input.

Finally, we note that equation (11) is almost certainly a large overestimate of the true conductivity, because a non-radial magnetic field, even a dynamically sub-dominant one, will greatly reduce the heat flux (Soker 1994). We address the effects of magnetic fields on conduction in more detail in Section 5.2. If the conductive heat flux is less than equation (11), then  $n_{\text{cond}}$  will shift to higher temperatures, thereby reducing the size of the forbidden region.

## 2.5 $L_{\text{dust}}$ : collisional heating of dust grains

The next energy sink we consider is the transfer of thermal energy from the hot gas to dust grains via collisions, followed by thermal radiation from the grains. The molecular clouds out of which MSCs form are dusty, and this dust can mix with the hot gas in two ways. First, the dust in ISM material can mix with the shocked wind material. Secondly, the expanding shell around the H II region will become corrugated with instabilities (Strickland & Stevens 1998), and the resulting turbulence at the hot–cold interface can mix dust grains into the hot gas. One final process by which dust can be supplied to and mixed with the hot gas is independent of the molecular cloud material: *in situ* formation of dust surrounding evolved stars such as red supergiants in the young MSC (Levesque 2010). Regardless of its source, dust grains immersed in hot gas will eventually be destroyed by sputtering, but they will absorb thermal energy via inelastic collisions and radiate it in the IR before that.

The importance of these processes depends on how well the dust is mixed with the hot gas and on how the sputtering and destruction time-scales compare (Smith et al. 1996; Draine 2011). These parameters depend on the properties of the dust grains and on the density and temperature of gas in the turbulent mixing layer. We address this question in detail in Section 5.3, but to be conservative we perform the calculation assuming that dust is able to survive in the hot gas with the same abundance as in the cold gas. Under this assumption, the gas–dust energy exchange rate by collisions with dust grains per unit volume of the hot gas is given by

$$\Lambda_{\text{gd}} = n_{\text{X}} n_{\text{d}} \sigma_{\text{d}} \left(\frac{8k_{\text{B}}T}{\pi m_e}\right)^{1/2} \bar{\alpha}_{\text{T}} (2k_{\text{B}}T_{\text{d}} - 2k_{\text{B}}T) \quad (14)$$

where  $n_{\text{d}}$  is the dust grain number density,  $T_{\text{d}}$  is the dust temperature,  $T$  is the hot gas temperature,  $\sigma_{\text{d}} = \pi a^2 \gamma_e$  is the dust cross-section where the factor  $\gamma_e$  allows for Coulomb focusing/repulsion of the hot electrons. Here,  $\bar{\alpha}_{\text{T}}$  is the averaged accommodation coefficient for an astrophysical mixture of gases which describes the fraction of kinetic energy of the impacting electron may be converted to heat (Burke & Hollenbach 1983; Draine 2011; Krumholz 2013). For dust grains immersed in hot gas with temperatures greater than  $\sim 10^6$  K, the electric potential is much less than the thermal energy of the impacting electrons, and thus, the dust grain can be treated as neutral (i.e.  $\gamma_e = 1$ ; Dwek 1987). We assume that the accommodation coefficient is equal for both H atoms and the hot electrons, with a value  $\bar{\alpha}_{\text{T}} = 0.3$  (Burke & Hollenbach 1983; Dwek 1987; Krumholz, Leroy & McKee 2011). For canonical values of the dust-to-gas mass

ratio and the dust grain cross-section, assuming that the total surface area of grains is proportional to the metal abundance, we find that the total energy exchange rate from the hot gas to the dust is

$$L_{\text{dust}} = \alpha_{\text{dg},e} n_{\text{X}}^2 V T^{3/2}, \quad (15)$$

where

$$\alpha_{\text{dg},e} = 2.20 \times 10^{-31} \frac{Z}{Z_{\odot}} \text{erg cm}^3 \text{K}^{-3/2} \text{s}^{-1} \quad (16)$$

is the grain–gas coupling parameter, which is proportional to  $n_{\text{X}}/m_e^{1/2}$  (Krumholz et al. 2011).

If heat exchange from the gas to the dust is primarily responsible for removing the bulk of the energy injected by winds, then the number density of the hot gas is

$$n_{\text{dust}} = \sqrt{\frac{L_w}{\alpha_{\text{dg},e} V T^{3/2}}}. \quad (17)$$

These results are also shown in Fig. 2 (dashed blue line). Again, the shaded region above this curve denotes the forbidden region within which the energy loss rate exceeds the injection rate.

Finally, we warn the reader that equation (15) is likely an overestimate of the true energy transfer rate of the hot gas colliding with dust. The value of  $\alpha_{\text{dg},e}$  is dependent on the adopted dust-to-gas ratio. Here, we have assumed that the dust-to-gas ratio for the hot gas is the same as that of the neutral ISM, where dust is perfectly mixed with the gas. The true dust-to-gas ratio in the hot gas is likely to be smaller, and the value will depend on the competition between turbulent mixing at the hot–cold interface and the sputtering of grains in the high-temperature medium.

## 2.6 $L_{\text{leak}}$ : physical leakage of the hot gas

The final energy sink that we will calculate is that associated with bulk motion of the hot gas. The hot gas may be only partially confined by the cold gas in the shell, either because the surrounding ISM is non-uniform or because stellar feedback punches holes in the shell. In either case, the hot gas, which has a much larger sound speed than the cool gas, will flow out of the holes, expand adiabatically, and cool radiatively (Harper-Clark & Murray 2009). In this scenario, the energy injected by stellar winds is ultimately radiated as low-surface-brightness X-ray and far-UV emission over an area much larger than the observed H II region.

Harper-Clark & Murray (2009) define a confinement parameter  $C_{\text{f}}$  that describes the ‘porosity’ of the cold shell, where  $C_{\text{f}} = 1$  describes a shell with no holes and  $C_{\text{f}} = 0$  describes a completely porous shell (i.e. no shell exists). The holes allow the hot gas to escape the H II region at its sound speed,  $c_{\text{s}}$ , with an energy flux given by

$$L_{\text{leak}} = (1 - C_{\text{f}}) 4\pi R^2 \frac{5}{2} \rho_{\text{h}} c_{\text{s}}^3, \quad (18)$$

where  $\rho_{\text{h}} = 1.9\mu_{\text{p}} n_{\text{X}}$  is the density of the hot gas,  $\mu = 0.62$  assuming He is fully ionized and its mass fraction is 0.3, and  $c_{\text{s}} = \sqrt{k_{\text{B}}T/\mu m_{\text{p}}}$  is the sound speed of the hot gas. Note that since  $L_{\text{leak}} \propto c_{\text{s}}^3$ , a large amount of leakage can occur even if the shell has a large covering fraction.

## 2.7 Other forms of energy loss

The energy losses by the mechanisms discussed previously in this section can be estimated easily under the stated assumptions. However, other avenues of energy loss also exist, including ‘turbulent

conduction' and 'turbulent work'. As we shall see below, the former mechanism may likely dominate the energy loss of the hot gas. Unfortunately, both channels are much harder to assess using observations, even at the order-of-magnitude level. None the less, we summarize these underlying physical mechanisms here.

Turbulent conduction (McKee et al. 1984) describes how cold gas can mix rapidly with hot gas via Kelvin–Helmholtz instabilities that occur as hot gas flows past cold clouds, either in the hot bubble interior or as it leaks out (Strickland & Stevens 1998; Nakamura et al. 2006). As with the estimate provided above for thermal conduction, this mixing will lead to rapid conductive transmission of the thermal energy, producing gas at temperatures of  $\sim 10^5$  K which sheds energy rapidly via metal-line cooling in the far-UV.

The difference between thermal conduction and turbulent conduction is that if a turbulent mixing layer is present, then the effective area of the hot–cold interface and the sharpness of the temperature gradient can be orders of magnitude larger than the laminar estimate given by equation (11). Moreover, if the turbulent mixing layer produces mixtures of hot and cold gas on scales smaller than the electron gyro radius, then magnetic confinement of the electrons will not be able to restrict the rate of energy interchange between hot and cold gas. Thus, the presence of a turbulent mixing layer might lead to a conductive loss rate much higher than the simple laminar estimate presented in Section 2.4.

The final energy loss mechanism we consider is turbulent work, where hot gas collides with the cold ISM and does work on it, converting its thermal energy into a turbulent cascade in the cold gas (Breitschwerdt & Kahn 1988). This process leads to the formation of shocks and to the energy being radiated in the IR (if dust cooling of the cold ISM dominates) or radio (if molecular line cooling dominates). Turbulent work is related to the mechanical luminosity we have estimated above, but it would manifest as large incoherent velocities rather than the coherent expansion in the previous estimate. It is unlikely that turbulent work would dominate over mechanical work because the total amount of work done on the cold ISM depends on the total surface area of the working surface (i.e. the bubble shell). As the shell expands coherently, the work done on the shell will be much greater than that over the turbulent regions. We therefore conclude that turbulent work is not a dominant energy sink for the hot gas.

### 3 H II REGION SAMPLE

#### 3.1 Sample selection criteria

In the previous section, we have reviewed the various physical processes that can contribute to the energy accounting problem. In the following sections, we derive constraints on the effectiveness of each process in depleting the injected wind energy from a sample of well-studied H II regions. We have selected this sample using several criteria. First, there must be X-ray data available to enable us to determine the physical properties of the hot gas and estimate the rate of radiative energy losses. Secondly, we require radio observations that allow us to characterize the dense shells bounding the H II regions, since the radius and velocity of this shell enter in our estimates for the mechanical luminosity.

Finally, we require robust observational estimates of the wind energy output by the stars. To obtain an accurate accounting of the wind energy, the spectral types of the majority of the luminous stars are necessary, so that star-by-star surface gravities and temperatures can be determined. Given these constraints, we have restricted our analysis to four well-studied H II regions in the LMC and MW, which

we describe briefly below. All our sources have young aged clusters ( $\sim 1$ – $3$  Myr old), and thus their X-ray emission is predominantly powered by stellar winds from their MSCs.

#### 3.2 Individual H II regions

##### 3.2.1 30 Doradus

30 Doradus (hereafter 30 Dor), located in the LMC (at a distance  $D \sim 50$  kpc), is the most luminous and largest H II region in the Local Group, with a radius of  $\sim 100$  pc and a bolometric luminosity of  $\sim 2.3 \times 10^8 L_{\odot}$  (Doran et al. 2013; Lopez et al. 2013b). It is primarily powered by NGC 2070 which contains  $\sim 2400$  OB stars. At its centre lies R136, a young ( $t_{\text{age}} \sim 1$ – $2$  Myr) dense star cluster with a stellar mass density of  $5.5 \times 10^4 M_{\odot} \text{pc}^{-3}$  (Parker 1993; Hunter et al. 1995). The total energy input by the stellar winds is  $2.2 \times 10^{39} \text{erg s}^{-1}$  (Doran et al. 2013), and its bubble shell is expanding at an average speed of  $\sim 25 \text{km s}^{-1}$  (Chu & Kennicutt 1994). The X-ray emission from 30 Dor was observed using the *Chandra* Advanced CCD Imaging Spectrometer (ACIS) for an integrated time of  $\approx 94$  ks (PI: L. Townsley). Lopez et al. (2011) found that the total diffuse unabsorbed X-ray luminosity of 30 Dor in the 0.5–2 keV band is  $4.5 \times 10^{36} \text{erg s}^{-1}$ . From the X-ray spectra, Lopez et al. (2011) found that the X-ray emission can be characterized by a hot plasma with a temperature of  $7.4 \times 10^6$  K.

##### 3.2.2 The Carina Nebula

The Carina Nebula, located at a distance of  $D \sim 2.3$  kpc, is one of the nearest regions of active massive star formation (Allen & Hillier 1993; Smith 2006). This complex is a 'cluster of clusters', containing eight open clusters. It hosts  $\sim 70$  O stars, of which 46 belong to the young star cluster Trumpler 16 ( $t_{\text{cl}} \sim 2$ – $3$  Myr; Smith 2006), the home of the well-known luminous blue variable  $\eta$  Carina. The total bolometric luminosity of the stars in the Carina Nebula is  $2.5 \times 10^7 L_{\odot}$ , and the total energy input by stellar winds is  $\sim 3.5 \times 10^{38} \text{erg s}^{-1}$ , with 70 per cent of the energy budget coming from Trumpler 16 (Smith 2006; Harper-Clark & Murray 2009). The nebula has a radius of  $\sim 20$  pc (Harper-Clark & Murray 2009; Townsley et al. 2011b) and its outer shell is expanding at a velocity of  $\sim 20 \text{km s}^{-1}$  (Smith et al. 2000; Smith & Brooks 2007). Carina has been studied extensively with *Chandra*. Townsley et al. (2011a) obtained a 1.2 Ms, 1.42 deg<sup>2</sup> ACIS-I mosaic of the complex to characterize its diffuse emission and to identify thousands of X-ray point sources (e.g. low-mass pre-main-sequence stars and massive stars). They found that the total integrated diffuse emission from the Carina Nebula in the 0.5–7 keV X-ray band is  $1.7 \times 10^{35} \text{erg s}^{-1}$ . To derive the temperature of the hot gas, Townsley et al. (2011b) fit the X-ray spectra with three non-equilibrium ionization plasma components. For our purposes, we assume that the observed hot gas temperature is the surface-brightness-weighted value taken from Townsley et al. (2011b). This yields a temperature of  $4.5 \times 10^6$  K.

##### 3.2.3 NGC 3603

The giant H II region NGC 3603, located at a distance of  $D \sim 7$  kpc, contains the most compact and youngest ( $t_{\text{cl}} \approx 1$  Myr) massive 'starburst' cluster located in the MW (HD 97950; Crowther & Dessart 1998). With a mass density of  $\sim 10^5 M_{\odot} \text{pc}^{-3}$ , HD 97950 is more compact than R136 (Hofmann, Seggewiss & Weigelt 1995). Assuming a distance of  $D \sim 8.4$  kpc (Goss & Radhakrishnan 1969), Balick et al. (1980) found that the radius of NGC 3603 (i.e. the region which

contains 90 per cent of the radio flux) is 25 pc. Assuming a distance of 7 kpc, the radius of NGC 3603 reduces to  $\sim 21$  pc. Balick et al. (1980) also studied the dynamics of NGC 3603 by measuring multiple emission lines, including H $\alpha$  and N II. They found that the N II lines are double peaked and separated by  $\sim 20$  km s $^{-1}$ . Furthermore, they also measured the velocity dispersion of the H $\alpha$  turbulent line widths to be 20 km s $^{-1}$ . These results suggest that NGC 3603 is expanding at a rate of  $\sim 20$  km s $^{-1}$ . Performing a stellar census of the massive stars in NGC 3603, Crowther & Dessart (1998) estimate that the total mechanical energy input by stellar winds is  $6.2 \times 10^{38}$  erg s $^{-1}$ . Smith (2006) suggest that the actual wind luminosity for NGC 3603 is smaller than this value because Crowther & Dessart (1998) do not consider the effect of wind clumping in their analysis. However, Smith (2006) does not quantify what this value is so we adopt the wind luminosity estimate from Crowther & Dessart (1998) and warn the reader that this may likely be an overestimate. NGC 3603 was observed with *Chandra* with 46 ks of usable time (Moffat et al. 2002). Townsley et al. (2011b) re-analysed these data and found 1328 X-ray point sources in the 17 arcmin  $\times$  17 arcmin ACIS-I field. After removing these point sources, Townsley et al. (2011b) found that the diffuse emission of NGC 3603 in the 0.5–7 keV band is  $2.6 \times 10^{35}$  erg s $^{-1}$ . Similarly to Carina, they fit the X-ray spectra by a multiple component plasma. Taking the surface-brightness-weighted average of their results, we adopt a hot gas temperature of  $6.2 \times 10^6$  K.

### 3.2.4 M17

The emission nebula M17, located at a distance of  $D \sim 2.1$  kpc, is on the eastern edge of a massive molecular cloud, M17SW, and exhibits a blister-like structure with a radius of  $\sim 5.8$  pc (Townsley et al. 2003). It is powered by the open cluster NGC 6616, which consists of a ring of seven O stars  $\sim 0.5$  pc in diameter (Townsley et al. 2003). NGC 6616 is quite young, with an estimated age of  $\lesssim 1$  Myr (Hanson, Howarth & Conti 1997). Assuming a distance of 2.1 kpc to the nebula, Hoffmeister et al. (2008) found that the total bolometric luminosity of the stellar population in M17 is  $3.8 \times 10^6 L_{\odot}$ . Dunne et al. (2003) estimate that  $L_w \sim 1 \times 10^{37}$  erg s $^{-1}$ . The bubble shell of M17 is expanding at a rate of  $\sim 25$  km s $^{-1}$  (Clayton et al. 1985). Townsley (2009) created a deep (total ACIS-I integration time of 320 ks) mosaic of M17. From these data, Townsley et al. (2011b) found that the total integrated diffuse emission from M17 in the 0.5–7 keV X-ray band is  $2.0 \times 10^{34}$  erg s $^{-1}$ . They modelled the X-ray spectra by a multiple component plasma, and from their model we adopt the surface-brightness-weighted value of  $5.3 \times 10^6$  K for the hot gas temperature.

## 4 RESULTS

In this section, we assess which sinks are responsible for removing the wind kinetic energy injected by MSCs in our four H II regions. We perform this analysis in several steps. First, in Section 4.1, we constrain the actual densities and temperatures of the hot gas in our sample H II regions using the available observations of their diffuse X-ray emission. Secondly, in Section 4.2, we evaluate all of the sink terms discussed in Section 2 to determine which of them, if any, might be responsible for removing the bulk of the wind energy. We use these calculations to evaluate the global energy budget for stellar wind energy injection in Section 4.3.

### 4.1 Observational constraints on the hot gas density and temperature

The density and temperature of the hot gas are jointly constrained by the observed (absorption-corrected) X-ray luminosity, while the temperature is constrained by the shape of the X-ray spectrum. We focus on the former constraint first. A ‘parcel’ of hot gas with temperature  $T$ , electron number density  $n_X$ , and volume  $V$  will have an X-ray luminosity given by

$$L_{X, \text{obs}} = 0.9n_X^2 V \int_{\nu_0}^{\nu_1} j_{\nu}(T, Z) d\nu, \quad (19)$$

where  $j_{\nu}(T, Z)$  is the emissivity of the hot gas and  $(\nu_0, \nu_1)$  is the frequency band of the X-ray telescope. For our purposes, we focus on the soft (0.5–2 keV) X-ray band when available, since the luminosity at these energies originates from the diffuse structures created by the collision of stellar winds. These are brighter by an order of magnitude than the point sources (Townsley et al. 2006). From the literature, we only have  $L_X$  for the 0.5–2 keV band for 30 Dor (Lopez et al. 2011), whereas we have  $L_X$  for the 0.5–7 keV band for the MW H II regions (Townsley et al. 2011b). We use CHIANTI to compute  $j_{\nu}(T, Z)$  for both MW and LMC abundances (Russell & Dopita 1992; Grevesse & Sauval 1998), and we show the results in Fig. 3. Under our simple assumption of a uniform hot gas filling the H II region, we can then combine the observed luminosity with the approximate volume of the region to obtain the number density of the hot X-ray emitting gas,

$$n_X = \sqrt{\frac{L_{X, \text{obs}}}{0.9V \int_{\nu_0}^{\nu_1} j_{\nu}(T, Z) d\nu}}. \quad (20)$$

From the X-ray data, one can also determine the temperature of the hot gas by modelling the X-ray spectrum as an absorbed hot diffuse gas. For this purpose, we adopt the surface-brightness-weighted temperatures derived from the observations, as discussed in Section 3.

Fig. 4 illustrates the locus in the  $T$ – $n_X$  plane allowed by the observed luminosities of our sample H II regions, with points marked along these curves corresponding to the temperatures inferred from the spectra. The  $n_X$  versus  $T$  curves for the MW sources have the

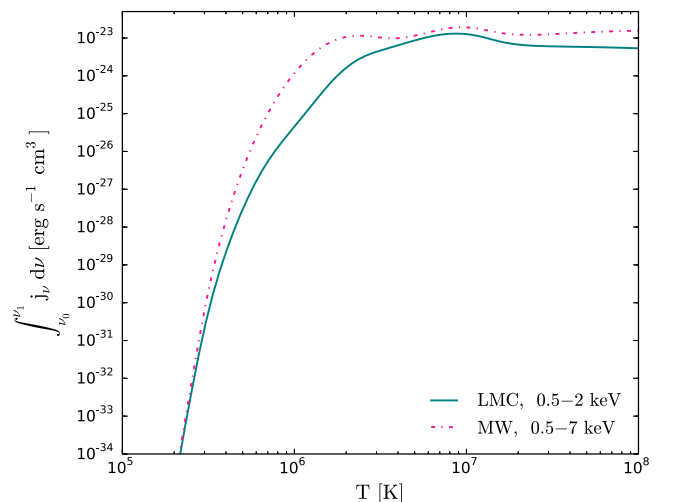


**Figure 3.** Frequency-integrated emissivities from CHIANTI for MW ( $Z = Z_{\odot}$ ) and LMC ( $Z = 0.5 Z_{\odot}$ ) metallicities assuming that the hot gas is in CIE. The LMC emissivity is integrated over the 0.5–2 keV *Chandra* band and the MW emissivity is integrated over the 0.5–7 keV *Chandra* band.

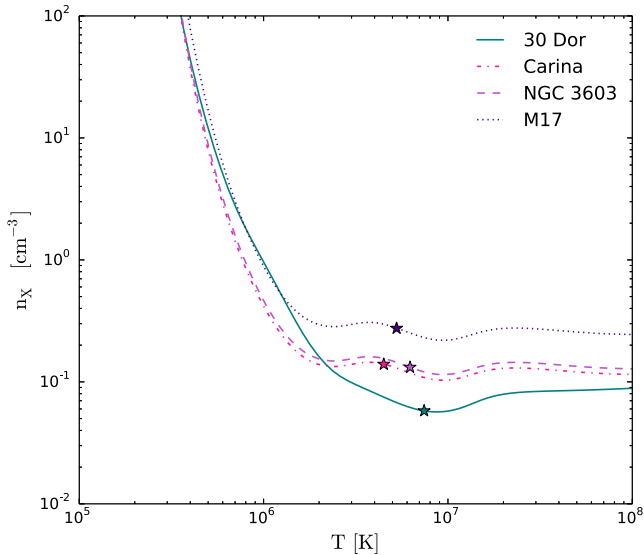


**Figure 4.** Allowed hot gas number density,  $n_X$ , versus temperature,  $T$ , constrained by X-ray observations for the 30 Dor, Carina, NGC 3603, and M17 H II regions. As can be seen, the allowed  $n_X$  for the MW H II regions (Carina, NGC 3603, and M17) follow the same shape but have different offsets due to their differing  $L_{X, \text{obs}}$ . The stars denote the temperatures inferred by spectral fitting (see Table 1).

same shape because they all use the same metallicity and bandpass for  $j_\nu(T, Z)$ , but have different observed luminosities. The curve for 30 Dor in the LMC has a slightly different shape due to the difference in both the frequency band used for the observations and in the gas metallicity.

## 4.2 Energy sinks

We next estimate the energy sinks discussed in Section 2 for our sample H II regions, in order to produce for each one a plot of the same type as shown in Fig. 2 (i.e. the loci in the  $T-n_X$  plane where each potential energy sink is capable of removing all of the kinetic energy injected by the winds). The inputs to these calculations are the observed H II region properties given in Table 1. We show the results of these calculations in Fig. 5, with the curves of  $n_X$  versus  $T$  inferred from the observed X-ray emission overlaid.

The  $L_{\text{cool}} = L_w$  curve (i.e. equation 4 – the solid teal line) indicates density–temperature combinations such that all the kinetic energy injected by stellar winds is radiated away. We remind the reader that the hot gas can only lie on or below  $n_{\text{cool}}$  line in order to conserve energy (i.e. the gas cannot radiate more energy than is injected into it). Clearly, the required number densities for cooling to dominate the energy loss are much larger than the number density constrained by the observed X-ray emission for all H II regions in our sample for  $T \gtrsim 10^6$  K. The observationally inferred gas temperatures are well above this limit. We conclude that radiative cooling is not an important energy sink, consistent with previous results (Dunne et al. 2003; Lopez et al. 2011; Townsley et al. 2011b).

Next, we consider the  $L_{\text{mech}} = L_w$  curve (i.e. equation 6 – the dot-dashed pink line), the locus of density–temperature combinations for which mechanical work on the dense shell removes the bulk of the wind energy. We find that for temperatures of  $\gtrsim 1-2 \times 10^6$  K, mechanical work becomes more efficient at removing energy since the hot gas pressure increases with temperature and  $L_{\text{mech}} \propto n_X$ . Thus, the  $L_{\text{mech}} = L_w$  curve requires lower number densities than radiative cooling to remove the wind energy. However, we find that  $n_{\text{mech}}$  is still larger than the number density constrained by the observed X-ray emission for all H II regions unless the hot gas

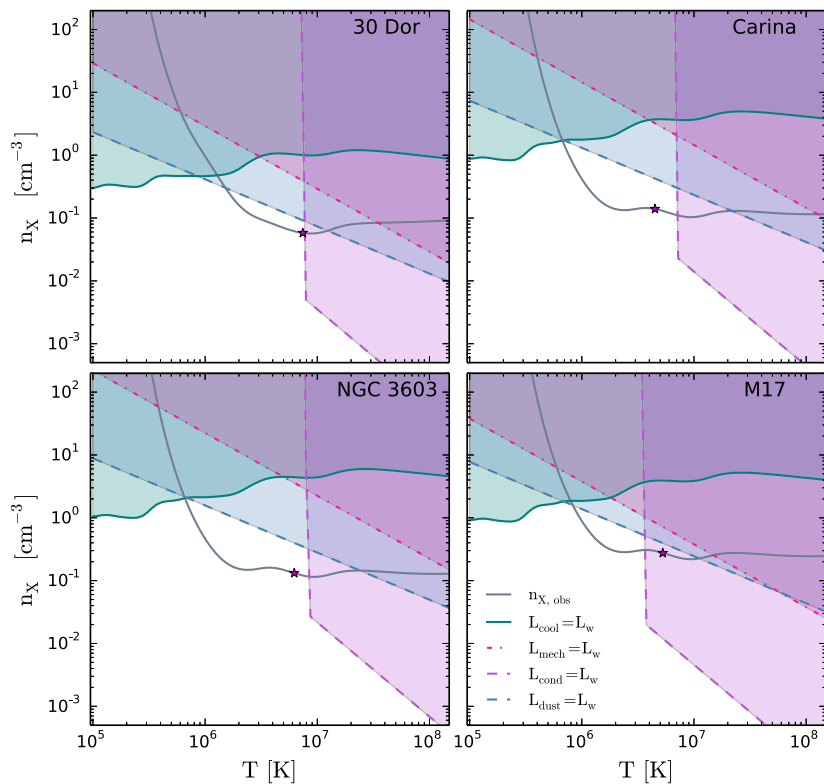


**Figure 5.** Same as Fig. 2 but for the H II regions in our sample. The grey lines with stars along them indicate the values of  $n_X$  versus  $T$  constrained by the observed X-ray luminosities, with the stars indicating the temperatures inferred by spectral fitting (see Table 1).

temperature exceeds  $\sim 0.2\text{--}1 \times 10^8$  K. None of the H II regions in our sample are in this temperature range. Thus, we conclude that mechanical work on the bubble shell is not responsible for removing the bulk of the wind energy.

The next energy sink we consider is thermal conduction. The  $L_{\text{cond}} = L_w$  curve (i.e. equations 12 and 13 – the dashed purple line) is nearly vertical at low temperatures because  $L_{\text{cond}}$  depends only weakly on density (e.g. equation 9) in the unsaturated regime. Only when the heat flux reaches the saturated value does the conductive luminosity exhibit any significant density dependence. We find that the observationally constrained number densities and temperatures do lie in the region where conduction is capable of removing the bulk of the wind energy for 30 Dor and M17. However, we remind the reader that our estimate of the conductive heat flux is almost certainly a sizeable overestimate, as we have entirely neglected the effects of magnetic fields. Thus, our results show that for densities and temperatures consistent with observations, thermal conduction can be an important energy sink for stellar wind energy as long as it is not significantly inhibited by magnetic fields.

Lastly, we consider the energy transfer of the hot gas to dust via collisions. The  $L_{\text{dust}} = L_w$  curve (i.e. equation 17 – the dashed blue line) indicates the density–temperature combinations at which all of the energy injected by stellar winds is transferred to the dust via collisions with the hot gas. We find that the heating of dust is more effective at removing energy from the hot gas than cooling and mechanical work for  $T \gtrsim 10^6$  K. We also find that the  $L_{\text{dust}} = L_w$  curve is quite close to the observational constraint line  $n_{X, \text{obs}}$  for temperatures consistent with the observed spectrum in 30 Dor and

M17. This result suggests that dust heating could be a significant energy sink for 30 Dor and M17, but probably not in NGC 3603 and Carina. However, as with conduction, our energy loss estimates for dust heating are likely to be large overestimates, since they assume that the dust content in the hot gas matches that in the cool ISM.

We defer a calculation of the rate of energy leakage via bulk motion to Section 4.4 since the confinement factor  $C_f$  is unconstrained observationally.

### 4.3 Implications for the energy budget

In order to better constrain the dominant source of kinetic energy removal, and to illustrate the problem of the missing wind energy, we next calculate the various energy sinks as a function of the hot gas temperature. We perform this calculation at each temperature  $T$  by using the observed X-ray luminosity to calculate the corresponding density  $n_{X, \text{obs}}$  from equation (20). For each  $T$ – $n_{X, \text{obs}}$  pair, we then compute all the energy sinks discussed in the previous section: radiative cooling, mechanical work, thermal conduction, and dust heating via collisions, and compare the sum of these cooling rates to the wind energy input rate.

Figs 6–9 show the results. Given the uncertainties in the true rates of conductive and dust heating, we perform this calculation both excluding them (left-hand panels) and including them (right-hand panels). The top panels show the absolute values of the individual and total energy loss rates, whereas the bottom panels show the energy loss rates as a fraction of the total energy injection rate by stellar winds. We remind the reader that values above the horizontal

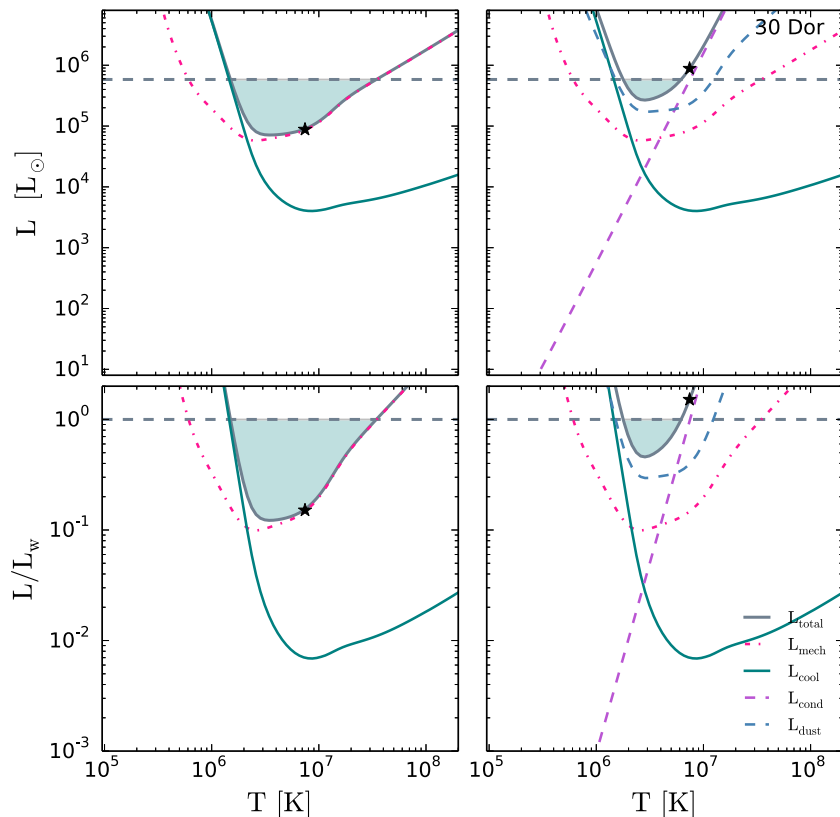


**Figure 6.** Hot gas temperature versus the energy loss rates for the energy loss mechanisms described in Section 2 for the observationally constrained hot gas number density for 30 Dor. The horizontal line in the top and bottom panels denote the stellar wind energy injection rate for 30 Dor. The left-hand panels consider only  $L_{\text{cool}}$  and  $L_{\text{mech}}$ , since these values are reasonable estimates whereas the left-hand panels also include thermal conduction and dust heating via collisions, which are likely overestimates. Stars denote the values of  $T_X$  inferred by spectral fitting.

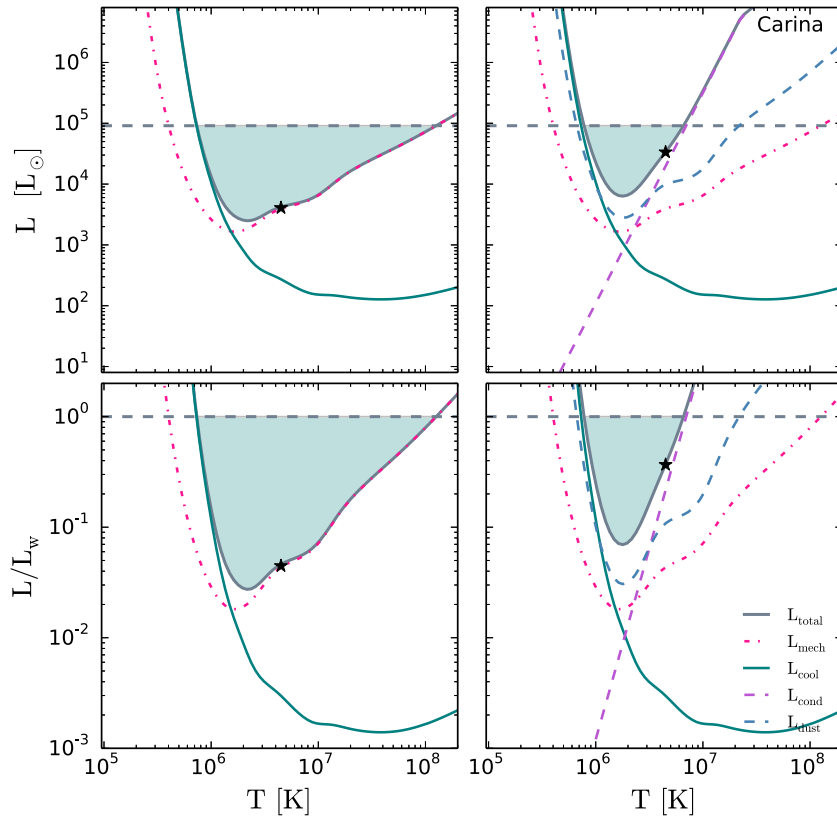


**Figure 7.** Same as Fig. 6 but for Carina.

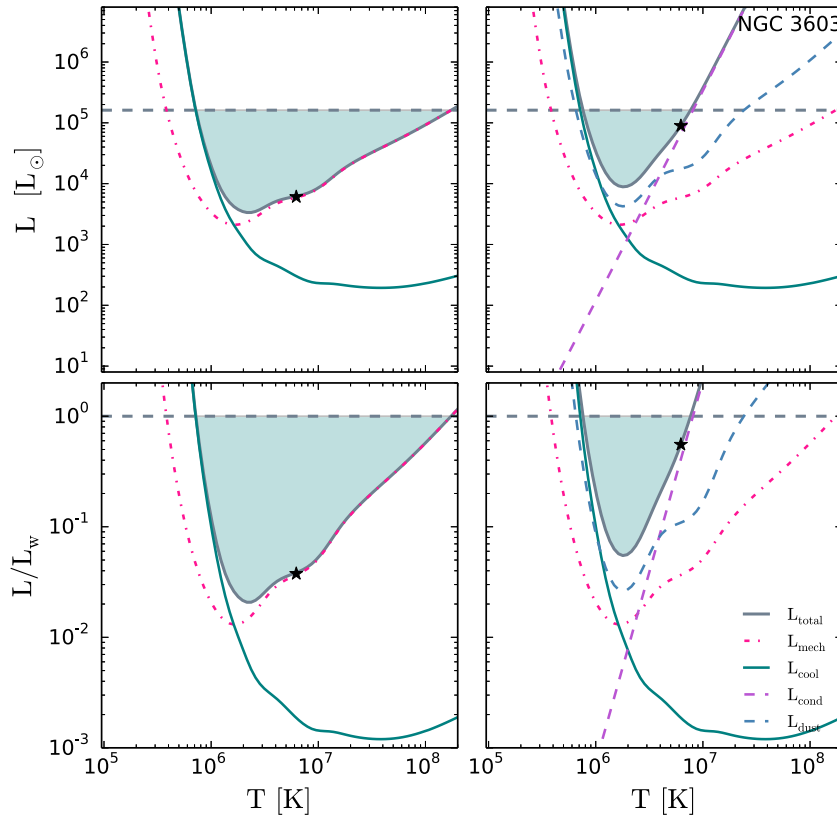


**Figure 8.** Same as Fig. 6 but for NGC 3603.

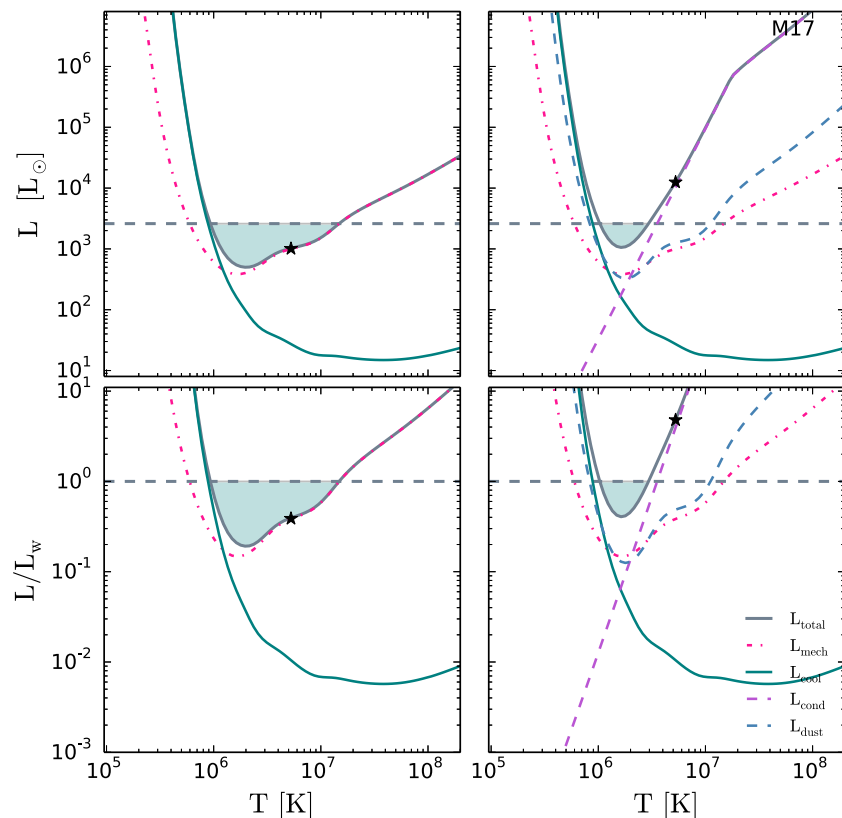


Figure 9. Same as Fig. 6 but for M17.

Table 2. Inferred number densities, luminosities, and confinement factors.

Name	$n_X$ (cm $^{-3}$ )	$L_{\text{cool}}/L_w$	$L_{\text{mech}}/L_w$	$L_{\text{cond}}/L_w$	$L_{\text{dust}}/L_w$	$C_f^a$	$C_{f,\text{all}}^b$
30 Doradus	0.058	0.37 per cent	15 per cent	<97 per cent	<40 per cent	>0.84	–
Carina	0.14	0.16 per cent	4.3 per cent	<22 per cent	<11 per cent	>0.36	<0.58
NGC 3603	0.13	0.10 per cent	3.7 per cent	<41 per cent	<11 per cent	>0.36	<0.70
M17	0.27	0.55 per cent	38 per cent	<392 per cent	<48 per cent	>0.95	–

Note. For each H II region in the sample,  $n_X$  is the number density inferred from the observed X-ray luminosity and best-fitting temperature. The columns  $L_{\text{cool}}/L_w$ ,  $L_{\text{mech}}/L_w$ ,  $L_{\text{cond}}/L_w$ , and  $L_{\text{dust}}/L_w$  show the radiative cooling, mechanical work, conduction, and dust cooling luminosities normalized to the wind energy injection rate; the latter two are upper limits. Finally,  $C_f$  ( $C_{f,\text{all}}$ ) is the confinement factor that would be required to remove the unaccounted-for wind energy via bulk motion.

<sup>a</sup>Derived  $C_f$  includes energy loss due to mechanical work and radiative cooling. These act as lower limits since the values obtained for these energy loss mechanisms are reasonable estimates.

<sup>b</sup>Derived  $C_{f,\text{all}}$  includes energy loss due to mechanical work, radiative cooling, thermal conduction, and dust heating via collisions. These act as upper limits since the values obtained for thermal conduction and dust heating via collisions are likely overestimates.

lines in these figures are not allowed due to energy conservation. The shaded regions illustrate how much energy is missing, i.e. what fraction of the injected wind energy cannot be accounted for by the sum of the various sinks we have been able to calculate. We also report these values, using the temperatures inferred from fitting the X-ray spectra, in Table 2.

For temperatures reasonably consistent with the observationally inferred values ( $4.5 \times 10^6 \text{ K} \lesssim T_{X,\text{obs}} \lesssim 7.5 \times 10^6 \text{ K}$ , cf. Table 1), we find that radiative cooling acts as a negligible energy sink, contributing to <1 per cent of the fractional energy loss for all H II regions. Mechanical work accounts for 3.7–38 per cent of the energy injected by winds, and for <15 per cent in three of our four sample regions. We find that mechanical work can account

for 38 per cent of the stellar wind energy injected in M17. This large fraction of energy transferred to mechanical work is likely due to M17’s small size. The inferred number density from the X-ray emission is inversely related to the H II region volume (i.e.  $n_X \propto V^{-1/2}$ ), thus a smaller volume for a given X-ray luminosity and plasma temperature would yield a larger inferred number density and hot gas pressure.

As illustrated in the right-hand panels of Figs 6–9, the situation is different if we include dust heating and/or thermal conduction. By combining these energy sinks with mechanical and radiative losses in Carina and NGC 3603, we can account for 37 and 55 per cent of the injected energy, respectively. In the remaining two H II regions, setting the conductive and dust cooling rates to their

maximum would lead to a luminosity greater than that injected by winds. However, this assumption is only true if magnetic fields do not inhibit conductive losses in any way and the dust to gas ratio is the same in the hot gas as in the cold ISM. Neither of those assumptions are likely to be true, as we discuss further in Section 5, even at the order of magnitude level. Only in M17, where we find  $L_{\text{cond}}/L_w \approx 4.8$  (see Table 2), is there a significant margin of error. In all the other regions, if the failure of these assumptions were to reduce the real conductive and dust luminosities by even a factor of a few compared to our upper limit, we would no longer be able to account for all the injected wind energy.

#### 4.4 Ways out: Where's the missing energy?

We have shown that the combined effects of radiative cooling and mechanical work cannot account for the missing energy of the hot post-shocked stellar wind material in our sample. Thermal conduction and dust heating via collisions might, but only if the assumptions described above are true. Are there other ways out?

One possible solution is that the hot gas acts as an energy reservoir for the winds. If storage in the thermal energy of the hot gas is significant, and has been over the cluster's lifetime, then the present-day thermal energy of the hot gas is of order of the total energy that has been injected since the winds started blowing,  $E_w \sim L_w t_{\text{cl}}$ . The resulting energy density for the stellar winds is  $u_w = L_w t_{\text{cl}}/V$ . Equating the stellar wind energy density to the energy density of the hot gas,  $u_X = \frac{3}{2}(1.9n_X T)$ , yields a number density of

$$n_w = 0.05 \left( \frac{L_w}{10^{38} \text{ erg s}^{-1}} \right) \left( \frac{t_{\text{cl}}}{\text{Myr}} \right) \left( \frac{T}{10^7 \text{ K}} \right)^{-1} \left( \frac{R_{\text{sh}}}{50 \text{ pc}} \right)^{-3}. \quad (21)$$

Assuming that the wind energy is stored in the thermal energy of the hot gas, we find that the required  $n_w$  is 0.6, 17, 8.4, and  $6.4 \text{ cm}^{-3}$  for 30 Dor, Carina, NGC 3603, and M17, respectively, for  $T = 5 \times 10^6 \text{ K}$ , roughly the observationally inferred value. Fig. 5 shows that these number densities are well above the observationally constrained  $n_X-T$  curve and well into the forbidden region where one or more loss mechanisms would remove energy faster than it is injected. This immediately demonstrates that depositing the wind energy into the thermal reservoir of the hot gas is not a viable solution.

Since the above argument suggests that the wind energy is not stored in the hot gas another possible solution is physical leakage of the hot gas. If the bubble shell is porous, the hot gas can physically leak out since the sound speed of the hot gas is greater than the expansion rate of the bubble shell (as discussed in Section 2.5). The energy loss by physical leakage is controlled by the porosity of the bubble shell, which we can parametrize by the covering fraction  $C_f$ . If the shell is very porous, the shock-heated gas will escape easily, resulting in a significant loss of the wind energy from the bubble, greatly reducing the X-ray luminosity. From the energy loss processes discussed in Section 2, we have that the total energy loss of the hot gas is

$$\frac{dE}{dt} = L_w - L_{\text{cool}} - L_{\text{mech}} - L_{\text{cond}} - L_{\text{dust}} - L_{\text{leak}}. \quad (22)$$

Using equation (18) and assuming that these processes account for the total energy loss of the hot gas (i.e.  $\frac{dE}{dt} = 0$ ),  $C_f$  is given by

$$C_f = 1 - \frac{2 [L_w - L_{\text{cool}} - L_{\text{mech}} - L_{\text{cond}} - L_{\text{dust}}]}{4\pi R^2 \mu m_p n_X c_s^3} \quad (23)$$

which depends on both  $n_X$  and  $T$ .

Fig. 10 show contours of the values of  $C_f$  required to account for the missing energy as a function of hot gas density and temperature.

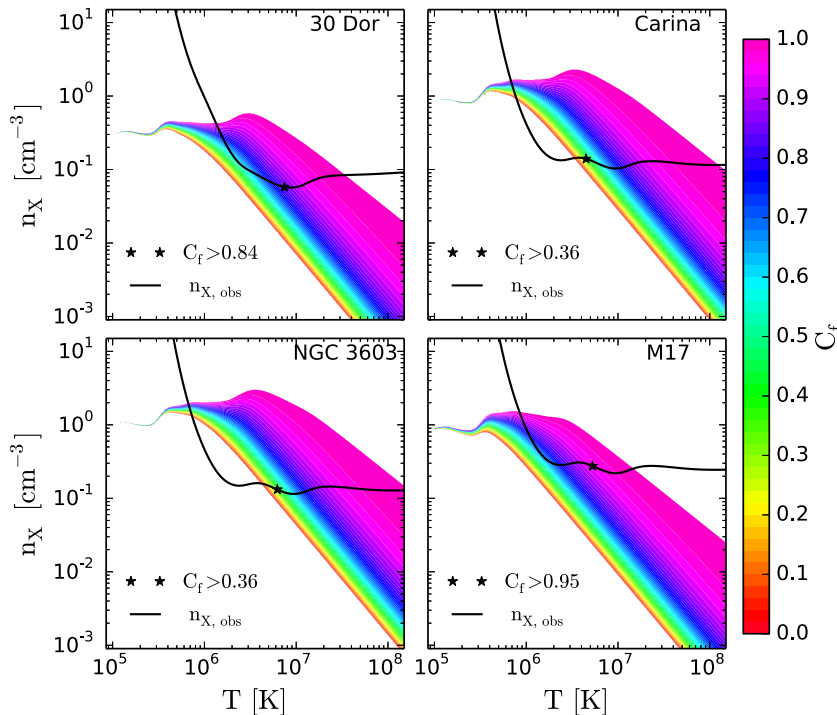


**Figure 10.** Contours of constant confinement parameter,  $C_f$ , for all H II regions in our sample. The value of  $C_f$  shown is that which would be required for physical leakage to account for all of the wind energy not removed by radiative cooling and mechanical work on the bubble shell. The curve of  $n_{X, \text{obs}}$  versus  $T$  required for consistency with the observed X-ray emission is overplotted. Stars denote the values of  $T$  inferred from the spectral fitting.

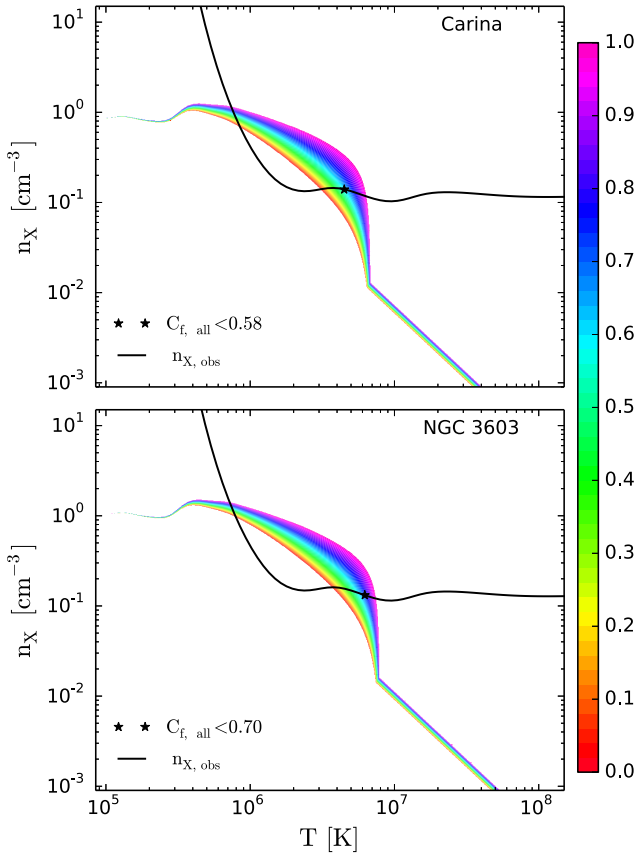


**Figure 11.** Same as Fig. 10 for Carina and NGC 3603 but also including the energy transfer associated with thermal conduction and collisional heating of dust grains.

To generate this figure, we solve equation (23) at each point in the  $T-n_X$  plane, assuming that only radiative cooling, mechanical work, and physical leakage contribute to energy loss, i.e. that  $L_{\text{cond}} = L_{\text{dust}} = 0$ . We also show the loci in the  $T-n_X$  inferred from the observed X-ray emission. The plot shows that physical leakage can adequately account for the missing energy for these H II regions for plausible values of the confinement factor. For the observationally favoured temperature and the corresponding derived density values (denoted by points in the figure), the required values of  $C_f$  are in the range 0.36–0.95 (also see Table 2). Adopting non-zero values of  $L_{\text{cond}}$  or  $L_{\text{dust}}$  would increase these values as can be seen in Fig. 11 and Table 2 for Carina and NGC 3603.

Finally, we note that there is one additional mechanism that we have not considered because we lack the ability to calculate it: turbulent mixing of the hot gas with cooler gas followed by conduction. As the shell expands into the ISM, the bubble shell interface becomes corrugated by instabilities (Strickland & Stevens 1998). These instabilities will lead to the addition of cooler, denser material in the bubble interior. This material can then mix with the hot gas, and the resulting large temperature variations over small scales will produce very rapid thermal conduction. For example, if the hot gas ( $T \sim 10^6 - 10^7$  K) mixes with the surrounding warm, ionized gas ( $T \sim 10^4$  K) the resulting mixture will have temperatures of  $\sim 10^5$  K (Dunne et al. 2003) and this gas will cool rapidly via metal-line cooling in the far-UV before adiabatically expanding and filling the whole H II region. Fig. 5 shows that the cooling of the denser, mixed gas can effectively radiate all of the wind energy.

## 5 DISCUSSION

### 5.1 Deviations from CIE

Throughout our analysis we have assumed that the post-shocked wind material responsible for the diffuse X-ray emission in H II regions is in CIE. This assumption allows one to easily determine the allowed locus in the  $T-n_X$  plane for an optically thin plasma given its observed X-ray luminosity. This is because the ionization fractions of the plasma depend only on  $T$  and  $Z$  under the assumption of CIE, as does the emissivity,  $j_\nu$ , and the radiative cooling function  $\Lambda$ . However, a hot plasma which was initially in equilibrium will deviate from equilibrium if the gas cools faster than it can recombine. The rapid cooling will cause the gas to become ‘overionized’ (Gnat & Sternberg 2007). One such example is if the hot plasma undergoes rapid adiabatic expansion before significant radiative losses can occur (Breitschwerdt & Schmutzler 1999) which has been observed in SN remnants (Lopez et al. 2013a, and references therein). This scenario is likely the case for the hot gas we are considering in MSCs because the initial post-shock wind material will adiabatically expand and fill up the entire H II region before suffering drastic radiative losses.

Gnat & Sternberg (2007) studied the time-dependent behaviour of a hot, low-density plasma and found that non-equilibrium effects cause the radiative cooling rate to be suppressed by a factor of 2–4 as compared to an equilibrium plasma. This result leads to an increase in the cooling time of a non-CIE plasma, rendering radiative cooling even more unimportant than our fiducial analysis suggests. Hence, our assumption of CIE likely only overestimates the cooling rate for a given density.

Similarly, the emissivity,  $j_\nu$ , integrated over the X-ray band, is of the order of  $\Lambda$  for the temperatures that we consider (e.g.  $T \gtrsim 10^6$  K). Thus, if  $\Lambda$  is suppressed by a factor of at most 4, then the integrated emissivity will decrease by a similar factor. This decrease in the emissivity will lead to the derived  $n_X$  to increase, at most, by a factor of 2, which would cause  $L_{\text{mech}}$  and  $L_{\text{dust}}$  to increase by factors of 2 and 4, respectively. Furthermore,  $L_{\text{cool}}$  will remain the same since the decrease in  $\Lambda$  will cancel the increase in  $n_X$ .  $L_{\text{cond}}$  will remain approximately the same since the energy loss due to conduction in the unsaturated regime depends very weakly on density. Hence, we conclude that if the hot gas is not in CIE then radiative cooling is still an inefficient energy sink for the hot gas. The energy transfer due to mechanical work on the shell and dust heating via collisions will be larger than our fiducial estimates, but only by factors of order unity.

### 5.2 Thermal conduction and magnetic fields

In our analysis, we found that thermal conduction can remove a significant amount of energy from the hot gas, but only if we assume that it is not substantially suppressed by the presence of a magnetic field oriented with field lines parallel to the wall of the bubble. If such a magnetic field is present, it inhibits electron transport between the hot and cold gas, reducing the conduction coefficient compared to our fiducial value by a factor of order  $(r_e/\ell_e)^2$ , where  $r_e$  is the electron gyroradius and  $\ell_e$  is the electron mean free path. In a plasma of  $10^7$  K gas with a density of  $1 \text{ cm}^{-3}$ , roughly our observationally inferred values,  $\ell_e \sim 0.04$  pc. In comparison, for a magnetic field of strength  $B$ , the gyroradius is  $r_e = 10^8 \sqrt{T_7/B_0}$  cm, where  $T_7 = T/10^7$  K and  $B_0 = B/1 \mu\text{G}$ , so the ratio  $(r_e/\ell_e)^2 \sim 10^{-20}$  even for an extremely weak field of  $1 \mu\text{G}$ . Thus, even such

a weak field will completely suppress conduction across field lines, and the only remaining question is the magnetic field geometry.

The molecular clouds out of which MSCs form are magnetized (Crutcher 2012). A number of authors have simulated H II regions expanding into magnetized media (e.g. Krumholz, Stone & Gardiner 2007; Arthur et al. 2011; Wise & Abel 2011; Gendev & Krumholz 2012), and a generic result of these simulations is that, as the H II region expands, advection of material out of the low-density interior into the surrounding swept-up dense shell results in a decrease in field strength in the H II region interior and an increase in field strength at the swept-up shell. This same phenomenon tends to reconfigure the field orientation such that, over most of the swept-up shell, the field is oriented parallel to the shell wall, i.e. the configuration that should be most effective at suppressing thermal conduction between the hot and cold phases. Although measuring magnetic fields in the shells that bound H II regions is difficult, there is some observational evidence for this phenomenon operating. Pellegrini et al. (2007) measure the field strength in the photodissociation region bounding the M17 H II region to be  $\sim 100 \mu\text{G}$ , far above the mean interstellar value, suggesting that field amplification has taken place and that conduction is being suppressed. Indeed, Dunne et al. (2003) conclude that such a strong field is required to explain the observed low X-ray luminosity of M17.

Although M17 is just one example, and in it we have only circumstantial observational evidence that the field is oriented parallel to the dense shell wall, that plus the simulation results is highly suggestive that magnetic suppression of conduction is probably very effective in most H II regions, with the effectiveness depending on the detailed magnetic field configuration. It is therefore likely that conduction is not a significant source of energy loss. Note that this statement does *not* apply to what we have termed turbulent mixing followed by conduction. The reason is that turbulence will cascade down to scales comparable to the electron gyroradius, and on such small scales, conduction is no longer suppressed by magnetic fields. Magnetic fields suppress only laminar conduction, not conduction that is the end product of a turbulent cascade originating at an unstable interface.

### 5.3 Dust sputtering and the dust cooling rate

We also found that the heating of dust by collisions with the hot electrons can be an important energy sink for the hot gas, but to be conservative we performed this calculation assuming the same dust to gas ratio in the hot gas as in the cold ISM. This assumption is unlikely to be satisfied. To see why, it is helpful to compare the mixing time-scale of the dust that is entrained into the hot gas with the time-scale for this dust to be destroyed by sputtering. The mixing time-scale will be of the order of the crossing time,  $\tau_{\text{cr}} = R/c_s$ , of the hot gas. In comparison, the approximate lifetime of dust grains immersed in hot gas is

$$\tau_d \approx 1 \times 10^5 \left[ 1 + \left( \frac{T}{10^6 \text{ K}} \right)^{-3} \right] \left( \frac{a}{0.1 \mu\text{m}} \right) \left( \frac{n_i}{\text{cm}^{-3}} \right)^{-1} \text{ yr}, \quad (24)$$

where  $a$  is the dust grain size (Draine 2011).

Fig. 12 shows the ratio of dust grain lifetimes and crossing times for the H II regions in our sample using our derived  $n_X$ , where we have assumed a typical grain size of  $0.1 \mu\text{m}$  in equation (24). We find that under our derived conditions, the dust grains will survive from a few  $\times 10^5$  years up to a couple Myr. This results in the dust surviving from a few to  $\sim 10$  crossing time-scales for

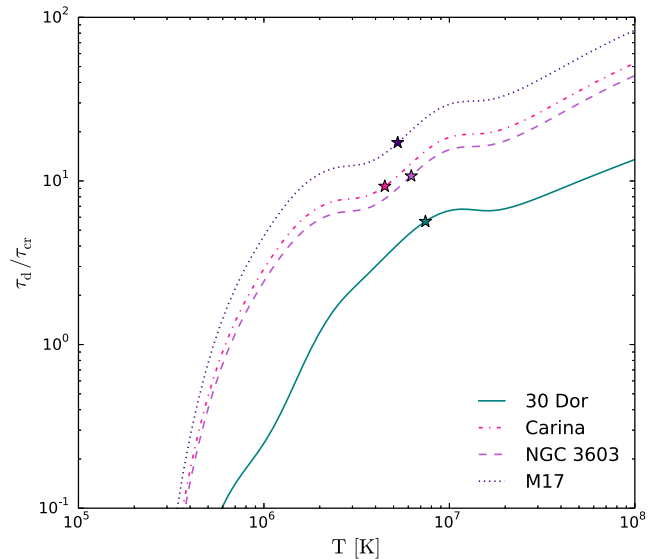


**Figure 12.** Ratio of the dust destruction time-scales to the crossing times for our H II region sample. The points denote the observed  $T_X$  and the corresponding  $n_X$  values obtained from our derived  $T-n_X$  plane.

the temperatures given in Table 1. This suggests that it is possible for dust grains with sizes greater than  $0.1 \mu\text{m}$  to survive for some length of time in the hot gas. However, since the crossing and destruction time-scales are not very different, our assumption that the dust abundance in the hot gas matches that in the cold gas is likely still a substantial overestimate. To keep the dust abundance so high, cold gas would have to be continually mixed into the hot H II region interior on times not much greater than the hot gas crossing time-scale. Such rapid mixing would likely in itself be a major cooling source, rendering the dust of secondary importance.

## 6 CONCLUSIONS

In this paper, we have examined the many different ways that MSCs can lose the kinetic energy injected by fast stellar winds from massive stars. These winds collide with each other and the ISM, generating hot shock-heated material at temperatures of  $\sim 10^7 \text{ K}$ , and the mechanical luminosity associated with the production of this gas is comparable to that provided by SNe at later stages of stellar evolution. However, the effects of this gas on the ISM depend critically on where the energy ultimately ends up – does it go into bulk motion of the cold ISM, possibly disrupting gas clouds and halting star formation? Is it radiated away as X-ray emission? Is it lost in some other way?

To address these questions, we have used the empirically determined properties from four LMC and MW MSCs. For each of these, the set of observational constraints is sufficient to allow us to estimate the wind energy input, and conversely, to estimate the rates of energy loss due to radiative cooling, mechanical work on the dense H II region shell, thermal conduction, collisional dust heating, and physical leakage of hot gas out of the dense shell. We find that radiative cooling of the hot gas accounts for less than 1 per cent of the total energy injected by stellar winds for the observed hot gas temperatures in the H II regions we have considered. While this might appear to favour a significant fraction of the energy going into mechanical work and thus being available as a form of feedback, our estimates of the rate of mechanical work on the dense H II region shell suggest that this is not the case. Instead, for all but one

of the H II regions (M17), we find that at most  $\sim 15$  per cent of the injected wind energy goes into doing mechanical work on the ISM. This limits the potential importance of winds as a stellar feedback mechanism, since it suggests that the efficiency with which they can be converted to bulk motion is fairly low.

This raises the question: If the bulk of the wind energy does not go into radiation nor mechanical work, where does it go? We identify four possible scenarios. The first is that the energy could be lost via thermal conduction at the hot–cold shell interface, followed by line radiation from this gas at far-UV wavelengths. However, this scenario appears to be viable only under the most optimistic possible assumptions. Thermal conduction will be dramatically reduced if there is a magnetic field parallel to the hot–cold interface, a configuration that simulations suggest should be common. It is possible to check this possibility via observations in several ways. If thermal conduction is the dominant loss mechanism, then observations of far-UV radiation in H II regions should discover a significant mass of  $\sim 10^5$  K gas in these objects. More indirectly, polarization studies and Zeeman line splitting measurements of the gas in H II regions and their shells can allow one to determine the orientation of the magnetic field and magnetic field strength. If the magnetic field is indeed parallel to the hot–cold interface, then thermal conduction will be strongly suppressed.

A second scenario is that wind energy stored in the hot gas is transferred to dust grains via collisions, and then radiated as infrared continuum. While this provides a sufficient energy sink to account for most of the injected wind energy if the dust content of the hot gas is the same as that of the cold gas, this too seems highly improbable. Grains  $\sim 0.1$   $\mu\text{m}$  in size will be destroyed by sputtering in the hot gas in a time that is only a factor of a few larger than the crossing time-scale, which suggests that it would be difficult to maintain a large population of such grains. Observationally, one might be able to evaluate this possibility by checking for distortions in the dust continuum spectrum. Since sputtering will preferentially destroy small grains, the infrared spectral energy distribution (SED) produced by the remaining grains should be shifted to longer wavelengths than the usual dust SED.

The third way the energy can be accounted for is if the hot gas physically leaks out of the H II region through holes in the bubble shell. These holes can be a result of stellar feedback punching holes in the dense H II region shell or because the shell expands into a non-uniform ISM. We find that, for plausible values of the confinement factor of the dense shell, this loss mechanism would be sufficient to account for the missing energy. In support of this scenario, Rogers & Pittard (2013) simulate the interaction of the mechanical energy input by stellar winds of three O-stars in a GMC and find that the hot gas generated by the shock heated stellar winds flows out of the GMC through low-density channels.

Our fourth and final scenario is that the hot gas can lose a significant amount of energy by mixing with the cold gas, followed by thermal conduction at the turbulent interface between the two – turbulent conduction. The resulting mixed gas will have temperatures of  $\sim 10^5$  K and will drastically cool via radiation in the far-UV. There is one indirect piece of observational evidence for this scenario: Bowen et al. (2008) report high O VI absorption in Carina, suggesting an overabundance of  $\sim 10^5$  K gas as compared to the normal ISM in the MW. Such an excess might also be evidence of laminar conduction without turbulent mixing, and one can distinguish between these scenarios by measuring the magnetic field strength and orientation. If a magnetic field parallel to the hot–cold interface is present, then the energy loss will most likely be dominated by turbulent conduction. We conclude that either this scenario

or physical leakage is the most likely explanation for the missing energy.

These four possible scenarios suggest that one productive avenue for further investigation is three-dimensional simulations of stellar wind feedback. Simulations of wind feedback including self-gravity and a realistically turbulent confining molecular medium are quite rare. Rogers & Pittard (2013) is one of the few examples. However, even these simulations include none of the physical mechanisms – magnetic fields, thermal conduction, dust sputtering – that would be required to address any scenario except bulk leakage. Incorporating these mechanisms into future simulations would be a valuable complement to observational studies such as this one, and might lead to the development of new observational diagnostics that could be used to track down the missing energy.

## ACKNOWLEDGEMENTS

ALR, MRK, and ERR acknowledge support from NASA through Hubble Archival Research grant HST-AR-13265.02-A issued by the Space Telescope Science Institute, which is operated by the Association of Universities for Research in Astronomy, Inc., under NASA contract NAS 5-26555. Support for this work was also provided by NASA through Chandra Award Number GO213003A and through Smithsonian Astrophysical Observatory contract SV373016 to MIT and UCSC issued by the Chandra X-ray Observatory Center, which is operated by the Smithsonian Astrophysical Observatory for and on behalf of NASA under contract NAS803060. ALR acknowledges support from the NSF Graduate Research Fellowship Program. MRK acknowledges support from NSF grant AST-0955300, and from NASA ATP grant NNX13AB84G. ERR acknowledges support from the David and Lucile Packard Foundation and NSF grant: AST-0847563. Support for LAL was provided by NASA through the Einstein Fellowship Program, grant PF1120085, and the MIT Pappalardo Fellowship in Physics. ALR thanks Chris McKee, Jason X. Prochaska, Leisa Townsley, Jorick Vink, and Jess Werk for useful discussions. We would like to thank our referee, Rolf Kudritzki, for a timely and detailed referee response and Prateek Sharma for his comments on VoxCharta.org.

## REFERENCES

- Allen D. A., Hillier D. J., 1993, *PASA*, 10, 338  
 Arthur S. J., Henney W. J., Mellema G., de Colle F., Vázquez-Semadeni E., 2011, *MNRAS*, 414, 1747  
 Balick B., Boeshaar G. O., Gull T. R., 1980, *ApJ*, 242, 584  
 Bowen D. V. et al., 2008, *ApJS*, 176, 59  
 Breitschwerdt D., Kahn F. D., 1988, *MNRAS*, 235, 1011  
 Breitschwerdt D., Schmutzler T., 1999, *A&A*, 347, 650  
 Bruhweiler F. C., Gull T. R., Kafatos M., Sofia S., 1980, *ApJ*, 238, L27  
 Burke J. R., Hollenbach D. J., 1983, *ApJ*, 265, 223  
 Cantó J., Raga A. C., Rodríguez L. F., 2000, *ApJ*, 536, 896  
 Castor J., McCray R., Weaver R., 1975, *ApJ*, 200, L107  
 Chevalier R. A., Clegg A. W., 1985, *Nature*, 317, 44  
 Chu Y.-H., Kennicutt R. C., Jr, 1994, *ApJ*, 425, 720  
 Clayton C. A., Ivchenko V. N., Meaburn J., Walsh J. R., 1985, *MNRAS*, 216, 761  
 Cowie L. L., McKee C. F., 1977, *ApJ*, 211, 135  
 Crowther P. A., Dessart L., 1998, *MNRAS*, 296, 622  
 Crutcher R. M., 2012, *ARA&A*, 50, 29  
 Cunningham A. J., Klein R. I., Krumholz M. R., McKee C. F., 2011, *ApJ*, 740, 107  
 Dale J. E., Ercolano B., Bonnell I. A., 2013, *MNRAS*, p. 587  
 Dere K. P., Landi E., Mason H. E., Monsignori Fossi B. C., Young P. R., 1997, *A&AS*, 125, 149

- Doran E. I. et al., 2013, *A&A*, 558, A134
- Draine B. T., 2011, *Physics of the Interstellar and Intergalactic Medium*. Princeton Univ. Press, Princeton, NJ
- Dunne B. C., Chu Y.-H., Chen C.-H. R., Lowry J. D., Townsley L., Gruendl R. A., Guerrero M. A., Rosado M., 2003, *ApJ*, 590, 306
- Dwek E., 1987, *ApJ*, 322, 812
- Fall S. M., Krumholz M. R., Matzner C. D., 2010, *ApJ*, 710, L142
- Gendele L., Krumholz M. R., 2012, *ApJ*, 745, 158
- Gnat O., Sternberg A., 2007, *ApJS*, 168, 213
- Goss W. M., Radhakrishnan V., 1969, *Astrophys. Lett.*, 4, 199
- Grevesse N., Sauval A. J., 1998, *Space Sci. Rev.*, 85, 161
- Hanson M. M., Howarth I. D., Conti P. S., 1997, *ApJ*, 489, 698
- Harper-Clark E., Murray N., 2009, *ApJ*, 693, 1696
- Hoffmeister V. H., Chini R., Scheyda C. M., Schulze D., Watermann R., Nürnberger D., Vogt N., 2008, *ApJ*, 686, 310
- Hofmann K.-H., Seggewiss W., Weigelt G., 1995, *A&A*, 300, 403
- Hunter D. A., Shaya E. J., Holtzman J. A., Light R. M., O’Neil Jr. E. J., Lynds R., 1995, *ApJ*, 448, 179
- Krumholz M. R., 2013, *MNRAS*, 436, 2747
- Krumholz M. R., 2014, *Phys. Rep.*, 539, 49
- Krumholz M. R., Matzner C. D., 2009, *ApJ*, 703, 1352
- Krumholz M. R., Tan J. C., 2007, *ApJ*, 654, 304
- Krumholz M. R., Stone J. M., Gardiner T. A., 2007, *ApJ*, 671, 518
- Krumholz M. R., Leroy A. K., McKee C. F., 2011, *ApJ*, 731, 25
- Krumholz M. R. et al., 2014, in Beuther H., Klessen R. S., Dullemond C. P., Henning T., eds, *Protostars and Planets VI*. Univ. Arizona Press, Tucson, AZ, preprint ([arXiv:1401.2473](https://arxiv.org/abs/1401.2473))
- Kudritzki R. P., Puls J., Lennon D. J., Venn K. A., Reetz J., Najarro F., McCarthy J. K., Herrero A., 1999, *A&A*, 350, 970
- Leitherer C., Robert C., Drissen L., 1992, *ApJ*, 401, 596
- Levesque E. M., 2010, *New Astron. Rev.*, 54, 1
- Lopez L. A., Krumholz M. R., Bolatto A. D., Prochaska J. X., Ramirez-Ruiz E., 2011, *ApJ*, 731, 91
- Lopez L. A., Pearson S., Ramirez-Ruiz E., Castro D., Yamaguchi H., Slane P. O., Smith R. K., 2013a, *ApJ*, 777, 145
- Lopez L. A., Krumholz M. R., Bolatto A. D., Prochaska J. X., Ramirez-Ruiz E., Castro D., 2013b, preprint ([arXiv:e-prints](https://arxiv.org/abs/e-prints))
- McKee C. F., Ostriker J. P., 1977, *ApJ*, 218, 148
- McKee C. F., van Buren D., Lazareff B., 1984, *ApJ*, 278, L115
- Matzner C. D., McKee C. F., 2000, *ApJ*, 545, 364
- Moffat A. F. J. et al., 2002, *ApJ*, 573, 191
- Murray N., Quataert E., Thompson T. A., 2010, *ApJ*, 709, 191
- Nakamura F., McKee C. F., Klein R. I., Fisher R. T., 2006, *ApJS*, 164, 477
- Parker J. W., 1993, *AJ*, 106, 560
- Pellegrini E. W. et al., 2007, *ApJ*, 658, 1119
- Pellegrini E. W., Baldwin J. A., Ferland G. J., 2011, *ApJ*, 738, 34
- Repolust T., Puls J., Herrero A., 2004, *A&A*, 415, 349
- Rogers H., Pittard J. M., 2013, *MNRAS*, p. 880
- Russell S. C., Dopita M. A., 1992, *ApJ*, 384, 508
- Smith N., 2006, *MNRAS*, 367, 763
- Smith N., Brooks K. J., 2007, *MNRAS*, 379, 1279
- Smith R. K., Krzewina L. G., Cox D. P., Edgar R. J., Miller W. W., III, 1996, *ApJ*, 473, 864
- Smith N., Egan M. P., Carey S., Price S. D., Morse J. A., Price P. A., 2000, *ApJ*, 532, L145
- Soker N., 1994, *AJ*, 107, 276
- Spitzer L., 1962, *Physics of Fully Ionized Gases*. Interscience Publishers, New York
- Stevens I. R., Hartwell J. M., 2003, *MNRAS*, 339, 280
- Strickland D. K., Stevens I. R., 1998, *MNRAS*, 297, 747
- Thompson T. A., Quataert E., Murray N., 2005, *ApJ*, 630, 167
- Townsley L. K., 2009, in Smith R. K., Snowden S. L., Kuntz K. D., eds, *AIP Conf. Proc.*, Vol. 1156, *The Local Bubble and Beyond II*. Am. Inst. Phys., New York, p. 225
- Townsley L. K., Feigelson E. D., Montmerle T., Broos P. S., Chu Y.-H., Garmire G. P., 2003, *ApJ*, 593, 874
- Townsley L. K., Broos P. S., Feigelson E. D., Brandl B. R., Chu Y.-H., Garmire G. P., Pavlov G. G., 2006, *AJ*, 131, 2140
- Townsley L. K. et al., 2011a, *ApJS*, 194, 1
- Townsley L. K., Broos P. S., Chu Y.-H., Gruendl R. A., Oey M. S., Pittard J. M., 2011b, *ApJS*, 194, 16
- Weaver R., McCray R., Castor J., Shapiro P., Moore R., 1977, *ApJ*, 218, 377
- Wise J. H., Abel T., 2011, *MNRAS*, 414, 3458

This paper has been typeset from a  $\text{\TeX}/\text{\LaTeX}$  file prepared by the author.